

# *Estimating LAI and uncertainty in grassland using UAV hyperspectral data and PROSAIL*

Zixiao Ding<sup>1,2</sup>, Xiaohua Zhu<sup>1</sup>, Lingling Ma<sup>1</sup>, Yongguang Zhao<sup>1</sup>

<sup>1</sup>National Engineering Laboratory for Satellite Remote Sensing Applications, Aerospace Information Research Institute, Chinese Academy of Sciences, Beijing, 100094, China

<sup>2</sup>University of Chinese Academy of Sciences, Beijing, 100094, China

**Keywords:** Leaf area index, Hyperspectral, PROSAIL, Uncertainty

**Abstract:** Leaf area index is an important structural parameter that characterizes vegetation growth conditions. Quickly and accurately obtaining the leaf area index of grassland vegetation can provide support for grassland ecosystem assessment and terrestrial carbon cycle research. Based on PROSAIL model and UAV hyperspectral data, this study established a LAI inversion model for natural grassland through feature band selection, PROSAIL parameter sensitivity analysis, lookup table combined with cost function. Through comparison with the measured data on the ground, the accuracy of LAI inversion was  $R^2=0.8289$ ,  $RMSE=0.3921m^2/m^2$ . Based on this, the possibility of improving the inversion model is proposed by analyzing the uncertainty of the image reflectance. After adding 5% Gaussian noise to ESI, the inversion accuracy is  $R^2=0.8394$  and  $RMSE=0.3900m^2/m^2$ , which proves the accuracy of uncertainty analysis.

## 1. Introduction

Leaf area index is defined as half of the total area of green vegetation leaves per unit surface area<sup>[1]</sup>, and is listed as one of the key parameters affecting global climate change by the Global Climate Observing System (GCOS)<sup>[2]</sup>. Hulunbuir Grassland has grazing and rest grazing periods every year, which will cause huge interference to the grassland ecosystem. Dynamic monitoring of changes in natural grassland is of great significance for studying the quality and quantity of grassland.

The current approaches to LAI inversion from hyperspectral images can be divided into statistical models and physical models. Compared with statistical models, physical models have a physical basis and are universal. PROSAIL is one of the most widely used physical models for LAI inversion<sup>[3]</sup>. Early scholars' research on leaf area index inversion using PROSAIL and other physical models mainly focused on forests and crops. For example, HeJinyou<sup>[4]</sup> combined artificial neural networks and PROSAIL models to invert forest LAI, proving that physical models have stronger universality than empirical models. Hao Xiaohui<sup>[5]</sup> used the PROSAIL model and genetic optimization algorithm to invert the LAI of soybean populations, and the correlation between the inverted values and the measured values was good. However, the applicability of UAV hyperspectral data combined with the PROSAIL model for LAI inversion of natural grassland remains to be studied. At the same time, after a series of processes such as radiometric calibration and atmospheric correction, UAV images have certain uncertainties in their image reflectivity. Uncertainty is propagated through the inversion

algorithm and has an inevitable impact on the final inversion result.

This paper uses the measured LAI and synchronized UAV hyperspectral remote sensing data of the grassland in the Hulunbuir during the growing season as data sources. Within the spectral range of the UAV hyperspectral sensor, a band-by-band combination method is used to extract the characteristic values. What's more, the maximum likelihood estimation method was used to conduct sensitivity analysis on the PROSAIL model, select sensitive parameters, use simulated spectra to establish a lookup table, and conduct LAI inversion of natural grassland based on the analysis of possible uncertainties in reflectance data.

## 2. Materials and methods

### 2.1 Study area

The research area is located in the Chinese Academy of Sciences Natural Grassland Restoration Experimental Area in the north of Hailar District, Hulunbuir City. ( $119^{\circ}28' \sim 120^{\circ}34' \text{ E}$ ,  $49^{\circ}06' \sim 49^{\circ}28' \text{ N}$ ). The study area and sample point distribution are shown in Fig 1. Summer in Hailar District is characterized by a large temperature difference between day and night and concentrated precipitation.

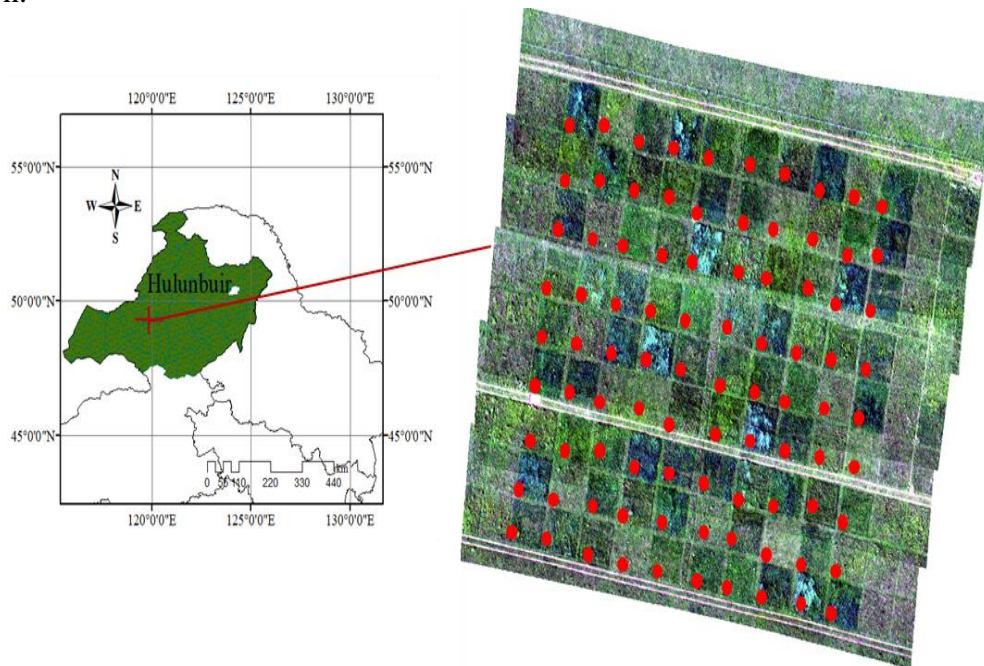


Figure 1: Distribution map of study area and sampling points

## 2.2 Data

### 2.2.1 LAI measurements

The field data used in this experiment were obtained through field measurements with the LAI-2200 vegetation canopy analyzer. A total of 90 quadrats were selected during the measurement, and a small quadrat of  $1\text{m} \times 1\text{m}$  was selected as the ESU (minimum sampling unit) in each quadrat. The measured sample points are divided into a training set and a verification set in a ratio of 5:4. The former is used to establish the inversion model, and the latter is used to verify the accuracy of LAI inversion.

### 2.2.2 UAV hyperspectral data

The hyperspectral sensor used in this experiment is Nano-Hyperspec. The sensor includes 272 bands in the range of 400~1000nm. The radiation resolution is 12-bit. After resampling, the interval is 2 nm. The spatial resolution of the acquired image is 0.083m.

## 2.3 Method

### 2.3.1 Hyperspectral feature selection

In order to screen out representative bands that can better invert the LAI of natural grassland, this study uses the band-by-band combination method to select characteristic bands of hyperspectral data, and uses the Pearson coefficient (R), which represents the fitting accuracy, to measure its correlation. The selected spectral index (SI) calculation formula is shown in Equations 1~5<sup>[6]</sup>.

$$NDSI = \frac{(R_i - R_j)}{(R_i + R_j)} \quad (1)$$

$$OSASI = \frac{(1+0.16) * (R_i - R_j)}{(R_i + R_j + 0.16)} \quad (2)$$

$$RDSI = (R_i - R_j) / \sqrt{(R_i + R_j)} \quad (3)$$

$$ESI = \frac{2.5 * (R_i - R_j)}{1 + R_i + 2.4 * R_j} \quad (4)$$

$$MSASI = \frac{2 * R_i + 1 - \sqrt{(2 * R_i + 1)^2 - 8 * (R_i - R_j)}}{2} \quad (5)$$

In Equations 1~5,  $R_i$  and  $R_j$  ( $i, j=1, 2, \dots, 272$ ) are the reflectivity of the  $i$  and  $j$ th bands.

### 2.3.2 PROSAIL sensitivity analysis

To provide comprehensive simulations of vegetation spectral response., PROSAIL combines two independent models, PROSPECT and SAIL. This study uses the PROSAIL model obtained by coupling PROSPECT-5B, the latest version of PROSPECT, with the SAIL model. Not only does it have many parameters, but due to spatial heterogeneity, its parameters cannot be directly applied to different regions. Therefore, it is necessary to perform sensitivity analysis on the parameters to complete the "localization" adjustment of the parameters.

Therefore, this experiment introduced GLUE<sup>[7]</sup> (Universal Maximum Likelihood Estimation) to evaluate the sensitivity of the PROSAIL model. The specific steps are as follows:

(1) Generate random parameter set

Based on the LOPEZ 93 (Leaf Optical Properties Experiment 93) database data and some references<sup>[8,9]</sup>, the value range of the 13 parameters in the PROSAIL model is set, and the size of the parameter set is set to 30000<sup>[10]</sup>. The parameter value range is shown in Table 1.

(2) Define likelihood criterion

In this study, the Nash coefficient, which reflects the degree of fit between simulated values and measured values, was selected as the likelihood criterion.

(3) Parameter sensitivity analysis

According to the assumed critical value, the parameter set is filtered, parameter combinations greater than the critical value are retained, and their likelihood values are normalized. Plot a scatterplot of the likelihood function values versus 12 parameters to find sensitive parameters.

Table 1: Parameter setting

Parameter	Abbr. in model	Unit	Range	Distribution type
Leaf structural parameter	N	Unitless	1~3	Uniform
Leaf chlorophyll content	C <sub>ab</sub>	ug/cm <sup>2</sup>	20~80	Uniform
Dry matter content	C <sub>m</sub>	g/cm <sup>2</sup>	0.002~0.02	Uniform
Equivalent water thickness	C <sub>w</sub>	g/cm <sup>2</sup>	0.002~0.04	Uniform
Brown pigments content	C <sub>brown</sub>	ug/cm <sup>2</sup>	0.02	/
carotenoid content	C <sub>ar</sub>	ug/cm <sup>2</sup>	8~20	Uniform
Solar zenith angle	tts	°	-30~30	Uniform
Viewing zenith angle	tto	°	-30~30	Uniform
Relative azimuth angle	Psi	°	0~180	Uniform
Leaf area index	LAI	m <sup>2</sup> /m <sup>2</sup>	1~6.5	Gaussian
Average leaf angle	ALA	°	30~80	Gaussian
Hot spot size parameter	hspot	m/m	0.05~0.5	Uniform
Soil brightness parameter	P <sub>soil</sub>	Unitless	0.1~1	Uniform

### 2.3.3 The look-up table (LUT) inversion

Different inversion algorithms differ in computational speed, robustness and performance. The most commonly used parameter inversion algorithms are numerical optimization algorithms, artificial neural networks (ANN) trained on RTM data, and look-up tables (LUT).

Compared with numerical iterative optimization and artificial neural networks, LUT provides a convenient method for LAI inversion. The advantages of the LUT method include the ability to avoid convergence to local minima, ease of operation, and high computational efficiency. Based on the above advantages, this study chose LUT combined with cost function as the inversion algorithm.

### 2.3.4 Uncertainty analysis

In LAI inversion, the most important input is surface reflectance. The uncertainty in image reflectance determines the accuracy of LAI inversion to a certain extent<sup>[11]</sup>. The optical signal measured by the UAV sensor needs to be converted into reflectance data through radiometric calibration and geometric correction, which introduces uncertainty in the reflectivity of UAV remote sensing images to LAI inversion. This study focuses on the impact of uncertainty in image reflectance on inversion.

Referring to Chen Wei<sup>[12]</sup> for the comparison of UAV hyperspectral data and spectrometer measured reflectance data, it is assumed that there is an uncertainty of 5% in the hyperspectral image. Select one simulated spectrum from each level I to V from the PROSAIL simulated spectral library for uncertainty analysis.

Monte Carlo simulation was used to add 5% Gaussian white noise to the two bands used to construct the vegetation index, and the number of simulations was 5000<sup>[13]</sup>. The noise-added

simulated spectrum was brought into the inversion model for LAI inversion, and 5000 The standard deviation of a group of LAI inversion values is used as the uncertainty of the group.

### 3. Results

#### 3.1 Feature selection

In order to screen out the band combination with the strongest correlation between Nano-Hyperspec hyperspectral data and LAI, Hulunbuir grassland LAI was used as the research object, and the band-by-band combination method was used for band selection. The band-by-band combination method uses any two bands of spectral data to construct NDSI, RSI, RDSI, ESI, and MSASI, and perform linear fitting with grassland LAI respectively. The results are shown in Fig 2.

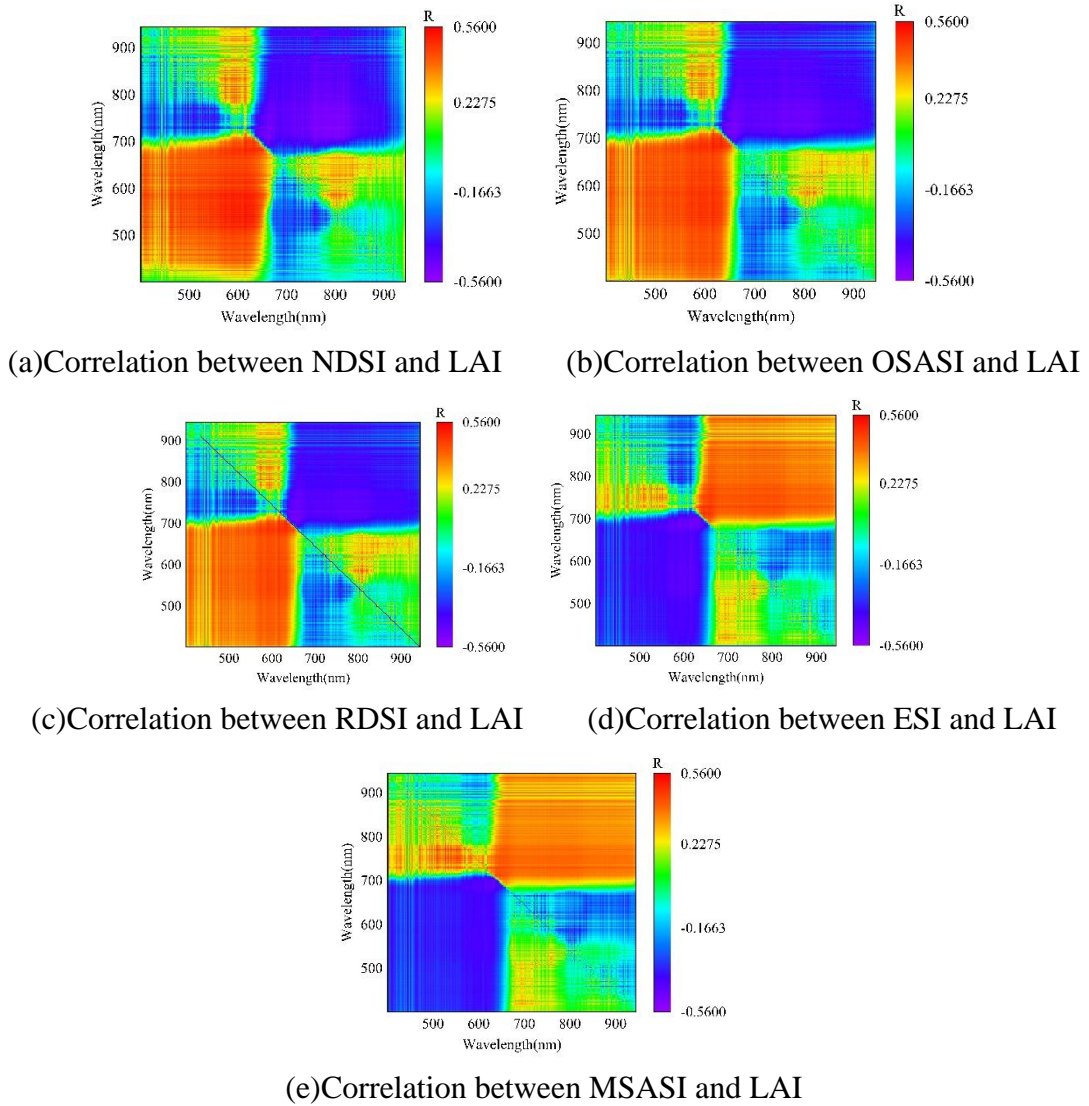


Figure 2: Correlation between each spectral index and LAI

As can be seen from Fig 2, NDSI (764, 555), OSASI (731, 744), RDSI (733, 746), ESI (728, 741), MSASI (862, 811) and LAI have the highest fitting accuracy, among the 5 Among the indices, NDSI has the strongest correlation with LAI, with the Pearson coefficient R being 0.5573. The R of the remaining four indices are 0.5206, 0.5206, 0.5131, and 0.5192 respectively. It can be considered that



the fitting accuracy of the characteristic band combination extracted by this method meets Experimental requirements <sup>[14]</sup>.

### 3.2 Sensitivity analysis and parameter adjustment of PROSAIL model

Among the 90 ground measured points sampled, LAI is distributed between 1.427 m<sup>2</sup>/m<sup>2</sup> and 6.107 m<sup>2</sup>/m<sup>2</sup>. Since GLUE needs to perform single-point analysis on PROSAIL, samples were taken from the LAI actual measurement points for single-point research. According to Yan Meiqi's<sup>[15]</sup> study on the correlation between LAI and FVC (Fractional Vegetation Cover), the equivalent relationship between grassland LAI and coverage (Equation 6) was established, and LAI was converted into coverage. LAI can be classified according to its coverage classification (Table 2).

$$y = 0.1194x + 0.1123 \quad (6)$$

In Equation 6, y is vegetation coverage and x is LAI.

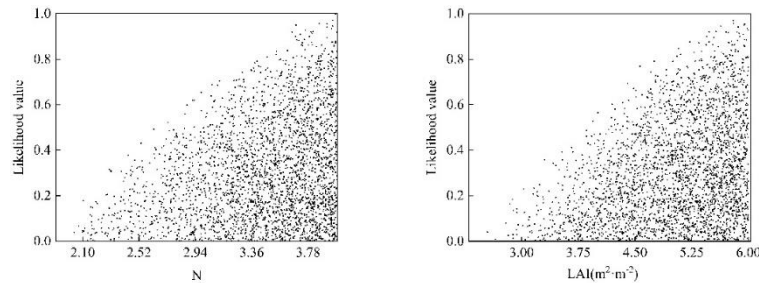
Table 2: Levels of vegetation sparsity

level	FVC	LAI
I	0<FVC<0.4	0< LAI <2.410
II	0.4<FVC<0.5	2.410< LAI <3.247
III	0.5<FVC<0.6	3.247<LAI <4.085
IV	0.6<FVC<0.8	4.085< LAI <5.760
V	FVC>0.8	LAI>5.760

According to Table 3, the LAI ground measurement points are divided into 5 levels, and a total of 5 sample points are randomly selected from the training set with reference to levels I-V for single-point research. Because the single-point sensitivity analysis of level II, III, IV, and V sample points is consistent with level I, only level I is listed here.

Taking 0.975 as the critical value, the parameter-likelihood value scatter distribution is obtained, and the relationship between parameter selection and likelihood value is analyzed. The parameters were divided into two categories based on the results.

The first category is sensitive parameters shown in Fig 3, whose parameter-likelihood value scatter plot has an obvious changing trend. Such parameters include leaf structure index N, chlorophyll C<sub>ab</sub>, leaf area index LAI, and average leaf inclination angle ALA. When considering the correlation between parameters, they are still relatively sensitive parameters. Based on their posterior distributions, the distribution type is changed to Gaussian distribution during inversion.



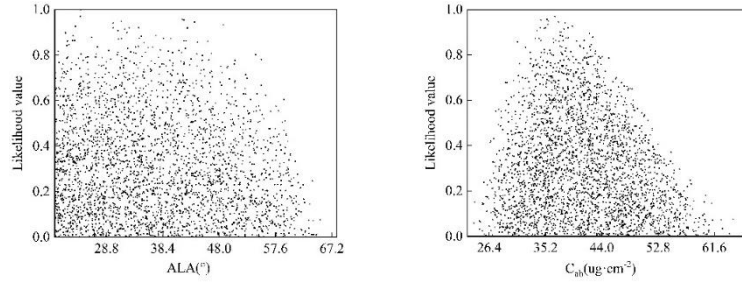


Figure 3: Sensitive parameters

The second category is insensitive parameters, such parameters include dry matter content  $C_m$ , hot spot parameter  $hspot$ , equivalent water thickness  $C_w$ , soil moisture index  $p_{soil}$ , carotene  $C_{ar}$ , solar zenith angle  $tts$ , observation zenith angle  $tto$  and relative azimuth angle  $psi$ . This is similar to the analysis result of Wang Lijuan. Subsequently, they are set to the mean of the current value range.

### 3.3 Inversion results based on UAV spectral

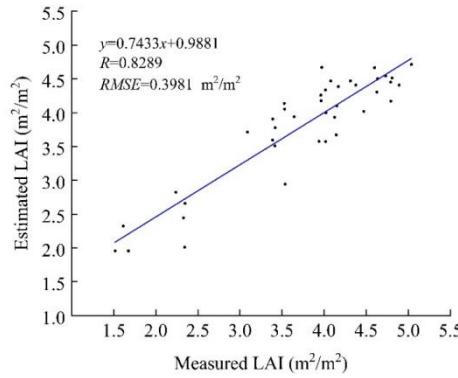


Figure 4: LAI inversion results

According to the study by Yun Jing<sup>[10]</sup> and others on the impact of lookup table size on LAI inversion accuracy, 30,000 parameter combinations of specific distributions were input into PROSAIL to obtain simulated spectra to construct a lookup table.

After the PROSAIL is driven by the above parameters to generate a lookup table, the UAV hyperspectral image is brought into the inversion model to perform LAI inversion and obtain the LAI inversion value. In order to verify the reliability of the inversion model, 40 sample point coordinates outside the modeling sample were brought into the inversion image, and the pixel values were extracted to obtain the LAI inversion value. The measured LAI is used as the reference true value and the LAI inversion value is used for regression analysis, and the correlation between the inversion value and the true value is obtained. The results are shown in Fig 4. It can be seen from Fig 4 that the LAI inversion  $R$  is 0.8289 and the RMSE is  $0.3981 \text{ m}^2/\text{m}^2$ . It shows that the inversion model is feasible for the inversion of LAI of natural grassland.

### 3.4 The impact of image reflectivity uncertainty on LAI inversion

#### 3.4.1 Simulated spectrum

In order to evaluate the impact of the uncertainty of different eigenvalues on the inversion, each eigenvalue of the five simulated spectra was inverted after adding noise. The standard deviation of

the inversion value is used as the uncertainty of the corresponding characteristic value of the simulated spectrum. The number of Monte Carlo simulations is set to 5000. The simulation results are as follows.

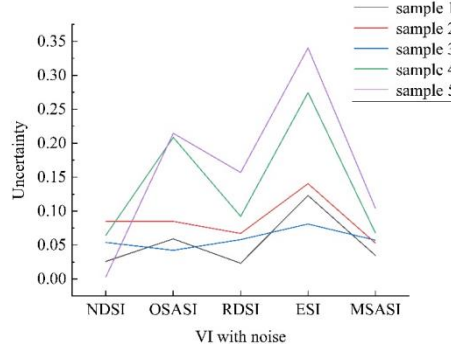


Figure 5: Uncertainty analysis

It can be seen from Fig 5 that after adding 5% Gaussian white noise to the five selected sample points, except for the NDSI group and OSASI group of sample point 2 and sample point 3, the performance trends are similar. And all five sample points fluctuate the most after adding noise in the two bands of EVI, and the uncertainty reaches the maximum value at this time. The wavelength bands used to construct the vegetation index are 728nm and 741nm, both of which belong to the red band. At this band, the vegetation spectral curve has an obvious phenomenon, namely the "red edge" phenomenon. The red edge is the point where the spectrum of green vegetation changes the fastest between 680nm and 740nm, and the 728nm band of the ESI after feature selection in this article is in this interval. In other words, under this parameter setting, the red edge position of the vegetation spectrum curve simulated by the PROSAIL model may be near the 728nm band, which will have the greatest impact on the inversion when the ESI changes.

### 3.4.2 Uncertainty Analysis of UAV Data

After uncertainty analysis of the simulated data, 5% Gaussian white noise was added to the UAV hyperspectral data in the same way and then entered into the inversion model. The results are shown in Table 3.

Table 3: Noise-added inversion results

Noise adding method	Noisy band	R <sup>2</sup>	RMSE
No noise added	/	0.8289	0.3981
NDSI Plus Noise	R764—R555	0.8231	0.4022
OSASI Plus Noise	R731—R744	0.8272	0.3968
RDSI Plus Noise	R733—R746	0.8318	0.3941
ESI Plus Noise	R728—R741	0.8394	0.3900
MSASI Plus Noise	R862—R811	0.8275	0.3996

As shown in Table 3, it can be seen that the inversion results after adding noise to each eigenvalue are quite different from the original inversion results. That is, when uncertainty exists in different bands, the impact on the inversion is different.

Among them, when it is assumed that there is uncertainty in the two bands of NDSI or MSASI, the LAI accuracy of the inversion decreases. The R<sup>2</sup> of the former decreases by 0.7% and the RSME increases by 1.0%. The R<sup>2</sup> of the latter decreases by 0.2% and the RMSE increases. 0.4%. If it is assumed that there is uncertainty in the two bands of OSASI, the LAI inversion result R<sup>2</sup> decreases by 0.2%, and the RMSE also decreases by 0.3%. When it is assumed that uncertainty exists in RDSI



and ESI, the LAI inversion accuracy can be improved. The former's  $R^2$  increases by 0.3% and the RMSE decreases by 1%. The latter's  $R^2$  increases by 1.3% while the RMSE decreases by 2.0%. Comparing the inversion results of the five eigenvalues, if it is considered that there is an uncertainty of 5% in the 728nm and 741nm bands of the hyperspectral image, the accuracy of LAI inversion which can be improved and a new method can be provided for natural grassland LAI inversion.

## 4. Conclusions

Understanding the growth status of natural grassland mainly depends on the physical and chemical parameters of grassland vegetation. As one of the key indicators for dynamic monitoring of vegetation growth, leaf area index is also closely related to the evaluation of ecosystems and plays a decisive role in the quality assessment of natural grassland.

Currently, LAI inversion with high spatial resolution mainly relies on ground measured data for modeling. This study divided the ground measured data into a training set to participate in modeling and a validation set to verify the inversion accuracy. Based on feature extraction, sensitivity analysis and lookup table fast inversion, a preliminary study was conducted on the impact of image reflectivity uncertainty on LAI inversion, and the following main conclusions were obtained:

(1) The band-by-band combination method can effectively extract UAV hyperspectral information. In addition to removing band redundancy, the bands with strong correlation with LAI inversion are retained. Among the five eigenvalues, NDVI has the strongest correlation with LAI, and the correlation coefficients of the other four eigenvalues are also higher than 0.5.

(2) GLUE was used as a global sensitivity analysis method to conduct sensitivity analysis on the PROSAIL model and determine the sensitive parameters and their distribution. 30,000 simulated spectra were simulated using the PROSAIL model, and fast inversion was performed through the lookup table. The  $R^2$  was 0.8289 and the RMSE was  $0.3981\text{m}^2/\text{m}^2$ , which proved the feasibility of the inversion model.

(3) The uncertainty brought by several possible situations of uncertainty in image reflectivity to LAI inversion was analyzed, quantified through Monte Carlo simulation, and the uncertainty under different situations was calculated. Among them, ESI brings a certain impact to the inversion. The greatest uncertainty comes. Based on the uncertainty analysis, Gaussian white noise is added to the image reflectance. Among them, after adding 5% Gaussian white noise to the two bands that make up the ESI, the accuracy of LAI inversion has been further improved, proving the reliability of uncertainty analysis.

## References

- [1] Asam S, Verrelst J, Klein D, et al. Leaf Area Index derivation from hyperspectral and multispectral remote sensing data in heterogeneous grassland[C]//9th EARSeL SIG Imaging Spectroscopy workshop.2015.
- [2] Duan S B, Li Z L, Wu H, et al. Inversion of the PROSAIL model to estimate leaf area index of maize, potato, and sunflower fields from unmanned aerial vehicle hyperspectral data[J]. *International Journal of Applied Earth Observations & Geoinformation*, 2014, 26:12-20.DOI:10.1016/j.jag.2013.05.007.
- [3] Pignatti S, Casa R, Harfouche A, et al. Maize Crop and Weeds Species Detection by Using Uav Vnir Hyperpectral Data[C]// IGARSS 2019 - 2019 IEEE International Geoscience and Remote Sensing Symposium. IEEE, 2019.DOI:10.1109/IGARSS.2019.8900241.
- [4] Pan Y, Wu W, Zhang J, et al. Estimating leaf nitrogen and chlorophyll content in wheat by correcting canopy structure effect through multi-angular remote sensing[J]. *Computers and Electronics in Agriculture*, 2023:208.
- [5] Singh M S. Hyperspectral Data-Based Waveform Parameters Response for Forest Leaf Area Index[J]. *Climate Change and Environmental Sustainability*, 2018, 6(1).
- [6] Song X N, Ma J W, Li X T, et al. Estimation of Vegetation Canopy Water Content Using Hyperion Hyperspectral Data[J]. *Spectroscopy & Spectral Analysis*, 2013, 33(10):2833.DOI:info:doi/10.3964/j.issn.1000-0593(2013)10-2833-05.

- [7] Zhu X , Li C , Tang L ,et al. Retrieval and scale effect analysis of LAI over typical farmland from UAV-based hyperspectral data[C]//Remote Sensing for Agriculture, Ecosystems, and Hydrology XXI.2019.DOI:10.1117/12.2535478.
- [8] Du R, Chen J, Xiang Y, et al. Incremental learning for crop growth parameters estimation and nitrogen diagnosis from hyperspectral data[J]. *Computers and Electronics in Agriculture*, 2023:215.
- [9] Wang L. Leaf Area Index Estimation Algorithm for GF-5 Hyperspectral Data Based on Different Feature Selection and Machine Learning Methods[J]. *Remote Sensing*, 2020, 12.DOI:10.3390/rs12132110.
- [10] Locherer M, Hank T, Danner M, et al. Systematic analysis of the LUT-based inversion of PROSAIL using full range hyperspectral data for the retrieval of leaf area index in view of the future EnMAP mission[J]. *IEEE*, 2015.DOI:10.1109/IGARSS.2015.7326705.
- [11] Daniel, Doktor, Angela, et al. Extraction of Plant Physiological Status from Hyperspectral Signatures Using Machine Learning Methods[J]. *Remote Sensing*, 2014.DOI:10.3390/rs61212247.
- [12] Chen H, Huang W, Li W, et al. Estimation of LAI in Winter Wheat from Multi-Angular Hyperspectral VNIR Data: Effects of View Angles and Plant Architecture[J]. *Remote Sensing*, 2018, 10(10):1630-. DOI:10.3390/rs10101630.
- [13] Sahoo R N, Rejith R G, Gakhar S, et al. Estimation of wheat biophysical variables through UAV hyperspectral remote sensing using machine learning and radiative transfer models[J]. *Computers and Electronics in Agriculture*, 2024, 221. DOI:10.1016/j.compag.2024.108942.
- [14] Zhao Y, Sun Y, Lu X, et al. Hyperspectral retrieval of leaf physiological traits and their links to ecosystem productivity in grassland monocultures[J]. *Ecological Indicators*, 2021, 122:107267. DOI:10.1016/j.ecolind.2020.107267.
- [15] Chen Q, Zheng B, Chen T, et al. Integration of APSIM and PROSAIL models to develop more precise radiometric estimation of crop traits using deep learning[J]. *Cold Spring Harbor Laboratory*, 2021.DOI:10.1101/2021.02.02.429471.